

Temporal metamaterials with passive switching as impedance-matched absorbers

Suat Barış İplikçioğlu

Department of Electrical and Electronics Engineering, Koç University

İstanbul, Türkiye

siplikcioglu15@ku.edu.tr

Abstract

Recent experiments on temporal reflection in transmission line metamaterials and theoretical treatments of dispersive time-varying media have unearthed the fundamental role of modulation mechanisms on the interface conditions, underpinning the introduction of passive photonic time crystals with stable momentum band gaps. Drawing from these concepts, it is shown that temporal metamaterials with simultaneous passive permittivity and permeability switching exhibit wideband absorption with impedance-matching, effectively behaving as one-dimensional perfectly matched layers. Under the effective medium theory, the loss mechanism is attributed to the emergent effective electric and magnetic conductivities, which are used to derive an approximate matching condition for asynchronous modulation and to engineer lossy material properties. The proposed approach and its performance beyond the Rozanov bound are verified with semi-analytical calculations as well as full-wave simulations, and the possibility of realizing a two-dimensional temporal perfectly matched layer is discussed.

1 Introduction

Dynamic control over temporal interfaces in complex media has unlocked a new regime of electromagnetic phenomena [1], ranging from parametric amplification [2] and inverse prisms [3] to temporal diffraction [4] and spatiotemporal wave control [5, 6]. To date, these interfaces have been explored across a diverse array of media, revealing complex rich physical behavior in plasmas [7, 8, 9, 10], Lorentzian media [11, 12, 13, 14, 15], chiral materials [16, 17], hyperbolic metamaterials [18, 19, 20] and non-Foster structures [21]. Beyond theoretical studies, temporal interfaces were experimentally realized with dynamic transmission lines in microwaves [22, 23, 24, 25] and with epsilon-near-zero materials under a pump-probe configuration in optics [4, 26, 27]. The impact of this paradigm extends beyond electromagnetics, with analogous temporal phenomena recently being observed in acoustic [28] and water waves [29].

The development of these time-varying systems has prompted a re-examination of the boundary conditions that characterize wave behavior at a temporal interface [30, 31]. Recent experiments on time-modulated transmission lines with passive switching of the distributed capacitance [22] have highlighted the validity of different boundary conditions during on- and off-switching [31, 32]. Within the context of unsteady plasmas and Lorentzian media, similar distinct boundary conditions were also derived to characterize wave dynamics during rapid ionization and charge recombination [8, 13, 14, 31, 33]. Concurrent with these interpretations of the temporal interfaces, the concept of passive photonic time crystals (PTC) with stable momentum band gaps was introduced for step-modulated transmission line metamaterials [34] and Lorentzian media [15].

This work demonstrates that a temporal metamaterial with impedance-matched passive permittivity and permeability switching, analogous to a dynamic transmission line medium, exhibits linear dispersion and constant loss profile without any momentum band gaps, showcasing properties similar to those of a one-dimensional perfectly matched layer (PML) [35]. Relying on high-frequency temporal modulations

in tandem with passive and reactive switching, the matched absorption mechanism presented herein is distinct from the previous time-variant configurations, which are based on backward wave cancellation [6, 25, 36], spectral redistribution/trapping of wave energy through single-shot switching [37, 38, 39, 40], coherent wave control [41, 42, 43], or resistive/active Floquet modulations [44, 45, 46, 47]. Furthermore, since the absorption is largely facilitated by high modulation frequencies, it does not require a phase synchronization with the incident waveform. An effective medium analysis [48, 49] of such materials is also shown to reveal effective electric and magnetic conductivities that can be used to engineer lossy material properties, as well as relaxed matching conditions for asynchronous modulation. The possibility of extending the approach to for the realization of a multidimensional PML is also theoretically evaluated. The results are verified with semi-analytical calculations and full-wave simulations.

2 Theory

2.1 Temporal interfaces in switched media

The main starting point of the analyses herein is the transmission line metamaterial medium. As in the conventional microwave theory [50], transmission line metamaterials can be modeled as simple LC ladders but with time-dependent distributed capacitances and inductances, which is equivalent to an isotropic medium with a capacitance-dependent permittivity and inductance-dependent permeability [51]. Capacitance modulation is achieved by opening or closing the switch between two parallel capacitors, whereas inductance modulation is performed through opening or closing a switch that shorts one of the two series inductors (Fig. 1). For the sake of simplicity, auxiliary resistances required for the physical realization of the switching transitions [32] are omitted from the unit cell model, and the switched reactive elements are assumed to have finite but sufficiently small internal resistances, such that their associated time constants are negligibly small. The case of capacitance or inductance increase can be treated by conventional flux continuity boundary conditions, as reported by Morgenthaler in 1958 [52]; nevertheless, the reverse case requires a first-principles treatment. When the parallel capacitor is switched off, bound charges are lost from the system, decreasing energy and momentum; such temporal interfaces can be represented with the continuity of voltage, rather than charge [31]. Importantly, a second switch should be connected to the auxiliary capacitor to discharge it after switching; thus, the remnant charges are not reintroduced to the system in case of periodic modulation. The dual problem is shorting of a series inductor with a closing switch: this case corresponds to the loss of magnetic flux linkage and can be represented by continuity of current, rather than magnetic flux. Alternatively, a switched metamaterial configuration can be constructed with a LC ladder of two parallel inductors and two series capacitors [32].

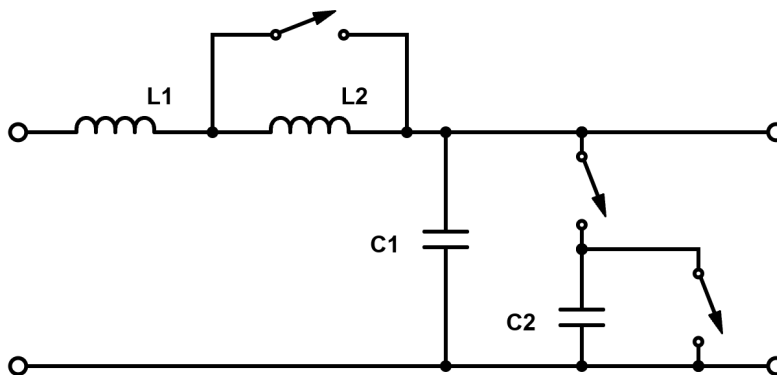


Figure 1: Unit cell of a transmission line medium under reactance switching with series inductors and parallel capacitors. The second switch on C2 acts to discharge the residual charges in between modulation.

Proceeding henceforth with analogous macroscopic electrodynamic quantities, the loss of charges and fluxes at a temporal interface with decreasing reactances at $t = t_0$ can be represented by an impulse of electric ($\mathbf{J} \propto \delta(t - t_0)$) and magnetic currents ($\mathbf{K} \propto \delta(t - t_0)$) [31]:

$$\int_{t_0^-}^{t_0^+} dt (\nabla \times \mathbf{E}) = - \int_{t_0^-}^{t_0^+} dt \left(\frac{d\mathbf{B}}{dt} + \mathbf{K} \right) = 0 \quad (1)$$

$$\int_{t_0^-}^{t_0^+} dt (\nabla \times \mathbf{H}) = \int_{t_0^-}^{t_0^+} dt \left(\frac{d\mathbf{D}}{dt} + \mathbf{J} \right) = 0 \quad (2)$$

The current terms can be alternatively decomposed as:

$$\mathbf{B}(t = t_0^+) - \mathbf{B}(t = t_0^-) = -\mu_0 \int_{-\infty}^{\infty} \Delta\mu\delta(t - t_0) \underbrace{\frac{1}{2} [\mathbf{H}(t = t_0^+) + \mathbf{H}(t = t_0^-)]}_{\mathbf{H}(t=t_0)} \quad (3)$$

$$\mathbf{D}(t = t_0^+) - \mathbf{D}(t = t_0^-) = -\varepsilon_0 \int_{-\infty}^{\infty} \Delta\varepsilon\delta(t - t_0) \underbrace{\frac{1}{2} [\mathbf{E}(t = t_0^+) + \mathbf{E}(t = t_0^-)]}_{\mathbf{E}(t=t_0)} \quad (4)$$

where $\Delta\varepsilon$ and $\Delta\mu$ are the absolute differences in relative permittivities and permeabilities, respectively. Thus, the impulsive electric and magnetic conductivities are in the form $\sigma(t) = \varepsilon_0\Delta\varepsilon\delta(t - t_0)$ and $\sigma^*(t) = \mu_0\Delta\mu\delta(t - t_0)$. For smooth temporal transitions, these can be represented as [31]:

$$\sigma(t) = \begin{cases} -\varepsilon_0 \frac{d\varepsilon(t)}{dt}, & \frac{d\varepsilon(t)}{dt} < 0 \\ 0, & \frac{d\varepsilon(t)}{dt} \geq 0 \end{cases} \quad (5)$$

$$\quad (6)$$

$$\sigma^*(t) = \begin{cases} -\mu_0 \frac{d\mu(t)}{dt}, & \frac{d\mu(t)}{dt} < 0 \\ 0, & \frac{d\mu(t)}{dt} \geq 0 \end{cases} \quad (7)$$

$$\quad (8)$$

2.2 Impedance-matched photonic time crystals and effective medium theory

It is known that under conventional temporal interface conditions [52], a nondispersive and active PTC under synchronous permittivity and permeability modulation exhibits a linear dispersion without momentum band gaps as long as the wave impedance is preserved throughout the modulation [53, 54]. In comparison, a passive PTC with synchronous and impedance-matched modulation exhibits a net loss while having closed momentum band gaps, which can be represented with complex frequency eigen-solutions in the form of $\omega = \omega_r + i\omega_i$ and $\omega_i < 0$ for all k . The loss mechanism can be understood first by focusing on a single unit cell of the periodic structure, e.g. a passive and matched temporal slab in a transmission line metamaterial. For this example, a concurrent increase in both capacitance and inductance scales down the forward wave amplitude without causing any backward waves, while a coordinated decrease after a time delay ensures that the amplitude remains constant. In both cases, the instantaneous energy density is reduced, while no reflections occur [32]. In electromagnetic terms, this can be interpreted by the effective material losses at the temporal interfaces: when passive switching is employed, the propagating waves are introduced to an impulse train of electric and magnetic conductivities at the falling edges of the modulation, which compensate for the gain and introduce loss. Under the well-known matching condition for transverse electromagnetic (TEM) waves [35], no instantaneous impedance discontinuities and hence no reflections occur for synchronous modulation of permittivity and permeability at the falling modulation edges:

$$\frac{\mu_0\mu_r}{\varepsilon_0\varepsilon_r} = \frac{\sigma^*}{\sigma} = \frac{\mu_0\Delta\mu}{\varepsilon_0\Delta\varepsilon} \quad (9)$$

Turning our attention to the exact eigenproblem for the time-periodic temporal slab, transfer matrix method (TMM) (Appendix A) reveals the closed-form dispersion relation to be:

$$\omega(k) = \pm kc_0 \frac{\varepsilon_1 \tau_2 + \varepsilon_2 \tau_1}{(\tau_1 + \tau_2) \varepsilon_1 \varepsilon_2} + \frac{2\pi m}{\tau_1 + \tau_2} + i \ln \left(\frac{\varepsilon_1}{\varepsilon_2} \right) \frac{1}{\tau_1 + \tau_2}, \quad \text{for } \varepsilon_2 > \varepsilon_1 \text{ and } m \in \mathbb{Z} \quad (10)$$

where ε_n and τ_n are the relative permittivities and their durations. It must be stressed that temporal decay of the matched PTC is linearly proportional with the switching period, whereas the permittivity/permeability ratio affects it logarithmically.

Since synchronous and completely impedance-matched modulation is not always possible due to jitter effects, oscillator detuning and/or difficulties in obtaining a large permeability change, a more relaxed matching condition can be obtained through the lens of effective medium theory (EMT). The effective constitutive parameters for the aforementioned two-phase medium are given as [48, 49]:

$$\varepsilon_{\text{eff}} = \left[\frac{1}{T_e} \int_0^{T_e} dt \frac{1}{\varepsilon_r(t)} \right]^{-1} = \frac{T_e \varepsilon_1 \varepsilon_2}{\varepsilon_1 \tau_{2e} + \varepsilon_2 \tau_{1e}} \quad (11)$$

$$\mu_{\text{eff}} = \left[\frac{1}{T_m} \int_0^{T_m} dt \frac{1}{\mu_r(t)} \right]^{-1} = \frac{T_m \mu_1 \mu_2}{\mu_1 \tau_{2m} + \mu_2 \tau_{1m}} \quad (12)$$

where $T_{e,m} = \tau_{1\{e,m\}} + \tau_{2\{e,m\}}$ is the modulation period of the each constitutive parameter. Similarly, homogenization of the impulse train of electric and magnetic conductivities yields:

$$\sigma_{\text{eff}} = \frac{1}{T_e} \int_0^{T_e} dt \sigma(t) = \frac{\varepsilon_0 \Delta \varepsilon}{T_e} \quad (13)$$

$$\sigma_{\text{eff}}^* = \frac{1}{T_m} \int_0^{T_m} dt \sigma^*(t) = \frac{\mu_0 \Delta \mu}{T_m} \quad (14)$$

Using Eqs. 11 to 14, the approximate matching condition (per Eq. 9) under the long-wavelength limit can be represented as:

$$\frac{\frac{\tau_{2e}}{\varepsilon_2} + \frac{\tau_{1e}}{\varepsilon_1}}{\frac{\tau_{2m}}{\mu_2} + \frac{\tau_{1m}}{\mu_1}} = \frac{T_e^2}{T_m^2} \frac{\Delta \mu}{\Delta \varepsilon} = Z_c^2 \quad (15)$$

where Z_c is the normalized wave impedance of the medium to be matched to. Besides matching, these effective medium parameters can be used to explain the behavior of passive PTCs with permittivity modulation, as well as to engineer dielectric or magnetic responses alongside loss in metastructures. This approach can also be interpreted as the effective medium generalization of the proposed formalism in [34], which designated duty cycle and impedance ratios as the characteristic variables for tuning momentum selectivity in passive PTCs. Significantly, the reciprocal of effective permittivity or equivalently permeability (Eqs. 11 and 12) appear directly on the dispersion relation for matched PTC (Eq. 10), indicating that the fundamental mode index is governed by the effective constitutive parameters. Nevertheless, the conductivity expression is still approximate and can be expressed exactly as:

$$\sigma_{\text{eff}} = \sigma_{\text{eff}}^* \frac{\varepsilon_0}{\mu_0} = -\varepsilon_0 \ln \left(\frac{\varepsilon_1}{\varepsilon_2} \right) \frac{\varepsilon_1 \varepsilon_2}{\varepsilon_1 \tau_2 + \varepsilon_2 \tau_1} \quad (16)$$

The behavior of passive PTCs in comparison with the active PTCs is documented on Fig. 2 with TMM and EMT. The constitutive parameters are assumed to be stepwise-modulated from 1 to 2 with a duty cycle of 0.5 and unity whenever time-invariant. An active PTC with permittivity modulation (Figs. 2a and 2b) exhibits a small momentum band gap with temporally growing ($\omega_i > 0$) and decaying solutions ($\omega_i < 0$). In the case of passive PTCs with permittivity-only modulation (Figs. 2c and 2d), the center Brillouin zone band gap is comparatively smaller; in addition, the dispersion relation exhibits a DC quasi-momentum band gap [34], whose effects can be attributed to the effective electric conductivity

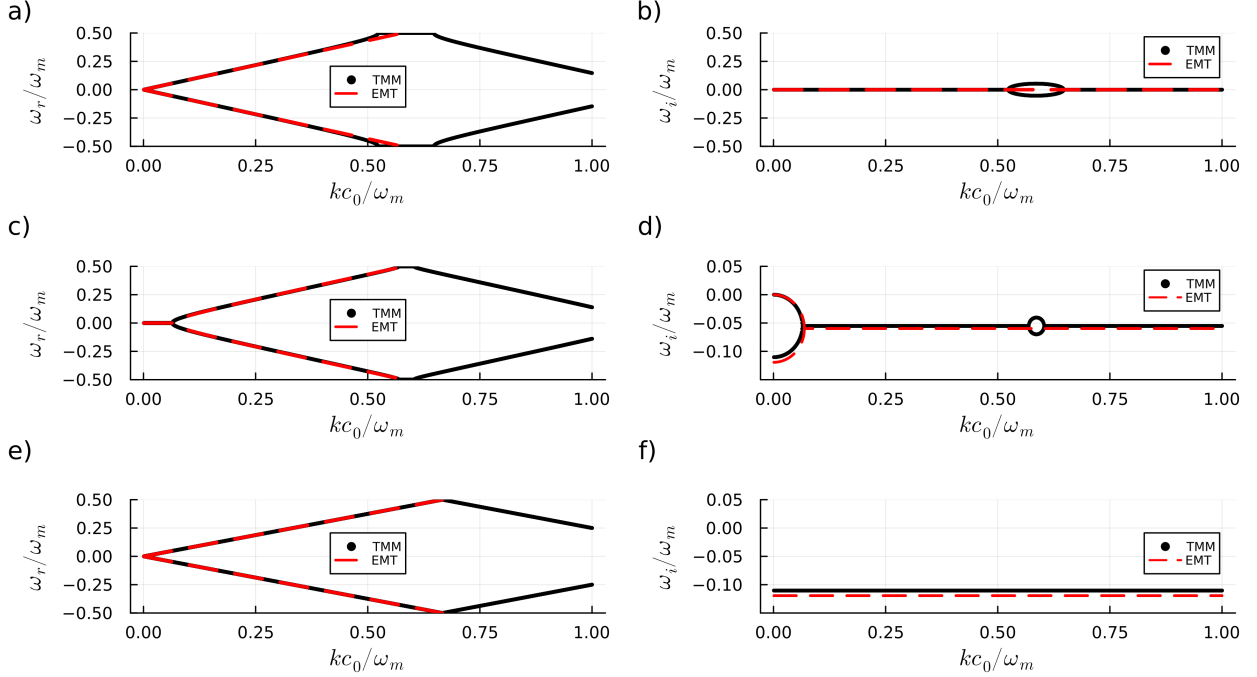


Figure 2: Band diagram of piecewise time-periodic media: a) Band diagram of an active PTC with permittivity modulation; b) temporal decay and growth in the active PTC; c) band diagram of a passive PTC with permittivity modulation; d) temporal decay in the passive PTC; e) band diagram of a passive PTC with impedance-matched modulation; f) temporal decay in the passive PTC with impedance-matched modulation

introduced by the switching. Per EMT, the dispersion relation of an arbitrary homogenized medium reads as:

$$\omega^2 \varepsilon_{\text{eff}} \mu_{\text{eff}} + \omega i \left(\frac{\sigma_{\text{eff}}^* \varepsilon_{\text{eff}}}{\mu_0} + \frac{\sigma_{\text{eff}} \mu_{\text{eff}}}{\varepsilon_0} \right) - \sigma_{\text{eff}} \sigma_{\text{eff}}^* c_0^2 = k^2 c_0^2 \quad (17)$$

For $\mu_{\text{eff}} = 1$ and $\sigma_{\text{eff}}^* = 0$, the solutions assume a purely imaginary form for $4k^2 \varepsilon_0 \varepsilon_{\text{eff}} \leq \mu_0 \sigma_{\text{eff}}^2$, forming the DC bandgap within this bound while having a stable temporal decay elsewhere; this also reproduces the PTC behavior outside the band gaps. In contrast, the band gaps completely close up in the case of a passive PTC with completely impedance-matched permittivity and permeability modulation, resulting in linear dispersion (Figs. 2e) and a constant temporal decay (Figs. 2f). When the temporal interfaces are no longer synchronized, the band gaps other than the DC band gap reemerge due to the reflections from impedance discontinuities within the temporal unit cell.

3 Impedance-matched absorption: results

In order to test the proposed absorption mechanism and effective medium models, wave interaction with a grounded slab (Dallenbach layer) under passive pulsed modulation is studied for normally-incident plane waves. The center frequencies of incident pulses were assumed to be 200 MHz. The step pulses are approximated with hyperbolic tangents, and a duty cycle of 0.5 as well as a lower permittivity/permeability bound of unity is adopted throughout the analyses, except where noted. The results are verified with semi-analytical Floquet expansion analyses and in-house finite-difference time-domain (FDTD) simulations, whose details are given on appendices B and C, respectively.

3.1 Matching under synchronous modulation

The spacetime profile of the electric field and reflectance of a grounded time-periodic slab of 0.2 m length is provided on Fig. 3. The modulation parameters are chosen as $\Delta\varepsilon = \Delta\mu = 4$ with $T_e = T_m = 1$ ns. Both modulation waveforms are synchronous ($\varepsilon(t) = \mu(t)$), which denotes a purely impedance-matched temporal metamaterial. The results for an incident Gaussian pulse showcase efficient absorption of the waves: on Fig. 3a, it can be observed that the incident wave encounters no significant impedance mismatch at the slab boundary at $z = 0$ and electric fields within the structure are rapidly attenuated at the falling edges of the modulation. Furthermore, reflectance of the Floquet harmonics are in line with the semi-analytical calculations, showcasing negligible higher-order reflections.

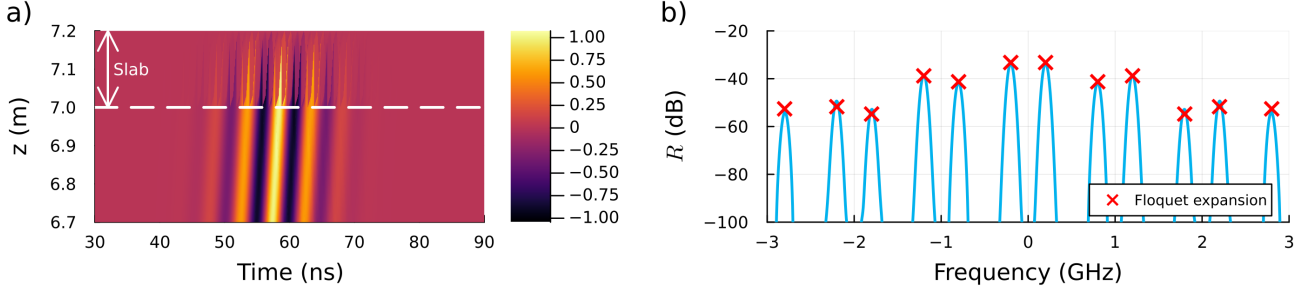


Figure 3: FDTD simulation of reflection from a grounded slab with impedance-matched permittivity and permeability switching: a) Spatiotemporal electric field profile; b) reflectance of Floquet harmonics.

3.2 Rozanov bound under passive switching

The performance of a grounded slab is governed by a fundamental trade-off between absorption efficiency, bandwidth, and thickness. This theoretical limit is quantified by the Rozanov bound [55], which defines the maximum achievable absorption for a given thickness and bandwidth:

$$\left| \int_0^\infty d\lambda \ln |\Gamma(\lambda)| \right| \leq 2\pi^2 \mu_r d \quad (18)$$

where $|\Gamma(\lambda)|$ is the wavelength-dependent reflection magnitude of the structure, μ_r is the relative permeability and d is the thickness. In practice, this bound, as well as the closely-related Bode-Fano limit, can be bypassed by linear time-varying systems using single-shot switching [37, 38, 39, 40] or periodic modulations [44, 45, 46, 47]. Thus, it is imperative to benchmark the absorption performance of the proposed mechanism in comparison with this fundamental limit.

In periodically time-varying systems, energy can be scattered into Floquet harmonics far outside the incident frequency band. Consequently, evaluating absorption efficiency based on a fully-defined incident spectrum is more physically insightful than relying on the traditional Rozanov integral (Eq. 18). This figure-of-merit is defined as [39, 46, 47]:

$$\eta_{\text{abs}} = 1 - \frac{\int_{-\infty}^{\infty} d\omega |E_{\text{ref}}(\omega)|^2}{\int_{-\infty}^{\infty} d\omega |E_{\text{inc}}(\omega)|^2} \quad (19)$$

where E_{ref} and E_{inc} are the reflected and incident electric field spectra, respectively. Since the original Rozanov bound is defined for band-limited signals in the wavelength space, rather than the frequency space as in Eq. 19, theoretical absorption limit is obtained numerically from the variational approach reported in [47]. Although the permeability of analyzed structure fluctuates in time, this absorption bound is evaluated using its peak value to establish a stringent and conservative upper limit. The

incident field is configured to have a flat and band-limited spectrum within the frequency space with $f = 200$ MHz and $\Delta f = 300$ MHz.

Fig. 4 illustrates the semi-analytically and numerically obtained absorption efficiencies alongside the Rozanov bound as well as the idealized results under EMT. The switching period for this example is chosen to be $T_e = T_m = 0.25$ ns to accentuate the modulation-induced effective conductivities within the layer; such sub-nanosecond switching speeds are physically realizable using high-speed step recovery diodes [40]. Noticably, the proposed mechanism exceeds the Rozanov bound for certain modulation depths. The static EMT results, representing an idealized PML, also surpass this theoretical bound significantly; this is physically permissible since effective magnetic conductivities, being absent from Eq. 18, remove the traditional upper limit on maximal absorption [56]. As the modulation depth increases, the calculated efficiency begins to deviate from the idealized EMT predictions, approaching the Rozanov bound. This can be attributed to the fact that homogenization overestimates the loss for larger $\Delta\epsilon$ and $\Delta\mu$. The absorption efficiency can further be increased under shorter switching periods, enabling beyond Rozanov performance with much smaller modulation depths.

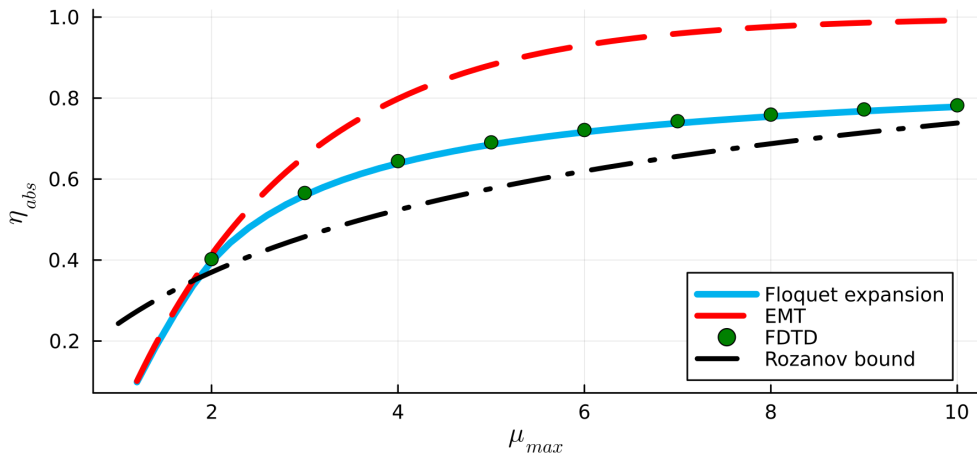


Figure 4: Absorption efficiency of a band limited signal with respect to the maximum permeability during modulation.

3.3 Matching under asynchronous modulation

In addition to synchronous impedance-matched modulation, the absorption performance under asynchronicity is also evaluated. The initial results are obtained for a half-space of switched medium to test the bounds of matching at the interface; asynchronicity for this specific case is achieved through introducing a time delay (T_d) between the permittivity and permeability functions. Reflectance data for the lowest-order harmonics is given on Fig. 5 for $T_e = T_m = 1$ ns. The FDTD results are obtained for a sufficiently thick slab of 15 m, ensuring convergence to the half-space results. Floquet expansion calculations predict essentially no reflection for the zeroth-order harmonic, whereas FDTD results exhibit a relatively small but finite reflection: this can be attributed to staircasing errors introduced by the Yee cell and decrease for smaller meshes. Evidently, interfacial reflection for lowest-order nonzero harmonics increases for longer time-delays. This behavior originates from instantaneous impedance discontinuities occurring within the temporal unit cell [53]. For a matched medium under synchronous modulation, the effective impedances seen by the Floquet modes are equivalent to the instantaneous wave impedance, which is unaltered at all times. When this staticity is broken by a time-delay, the higher-order modes encounter different characteristic impedance within the layer, which results in reflections. It is further observed that this mismatch is exacerbated by stronger modulation profiles, necessitating the use of alternative approaches in addition to the simple matching condition (Eq. 15).

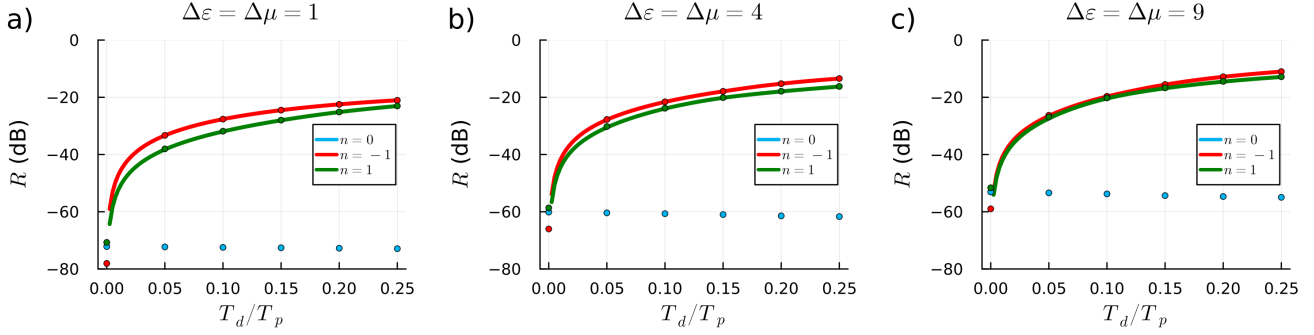


Figure 5: Reflectance of a time-varying half-space with respect to the time delay (T_d) between permittivity and permeability modulations and the modulation depth. Line and scatter plots show the Floquet expansion and FDTD results, respectively.

Nevertheless, impedance matching under the approximate relation in Eq. 15 can still be ensured as long as excitation of higher-order harmonics at the interface are sufficiently suppressed. This can be done through tapering the modulation depth across the layer, which itself is a widely-adopted technique for the numerical implementation of PMLs in FDTD method [35]. In order to test the bounds of tapered matching, we fix the periods of permittivity and permeability functions to 1 ns and $1/\sqrt{2}$ ns, respectively; this results in an almost-periodic PTC [57] with a strong detuning between the permittivity and permeability profile. The modulation depth of the permittivity is graded from zero a maximum value of 9 at the end of a slab of 1 m with a cubic grading. The corresponding duty cycle and modulation depth of the permeability function is obtained from the quasistatic matching condition in Eq. 15. The FDTD results are given on Fig. 6; these suggest that absorption levels similar to that of the synchronous switching can be obtained at the expense of a longer taper and a larger dielectric modulation depth. Furthermore, this also shows that bounds on the permeability change can be relaxed under a higher switching frequency.

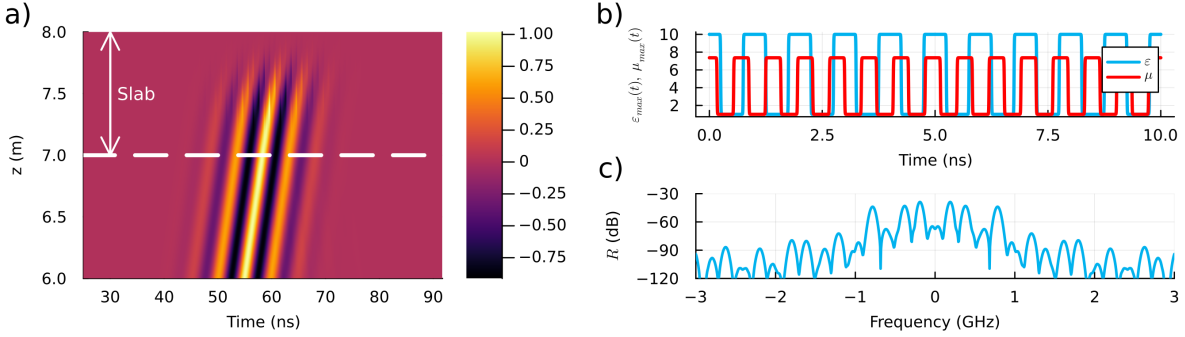


Figure 6: FDTD simulation of a grounded and tapered slab with asynchronous modulation and an almost-periodic instantaneous wave impedance: a) Spatiotemporal field profile; b) Time-domain permittivity and permeability functions at $z = 8$ m; c) spectral reflectance.

3.4 Reconfigurable material responses in the effective medium limit

Besides the matching mechanism discussed so far, passive temporal metamaterials under permittivity or permeability switching can be used to engineer arbitrary lossy material responses at desired frequencies. Validation of this effect is provided by the same grounded slab configuration as before, assuming purely dielectric material properties. Using transmission line theory [50], matching condition of this structure

in the effective medium limit is given as:

$$\sqrt{\varepsilon_c} \cot\left(\frac{\omega}{c_0} \sqrt{\varepsilon_c} d\right) + i = 0 \quad (20)$$

where ε_c and d are the complex relative permittivity and thickness, respectively. For $d = 0.2$ m, the target complex permittivity is obtained as $\varepsilon_c = 3.913 + i2.337$ through numerical optimization [58]. Per Eq. 13, the effective conductivity σ_{eff} and the necessary modulation depth $\Delta\varepsilon$ are given as $\text{Im}[\varepsilon_c]\omega\varepsilon_0$ and $\text{Im}[\varepsilon_c]\omega T_e$, respectively. Using the effective dielectric constant expression (Eq. 11), the real part of the complex permittivity ($\text{Re}[\varepsilon_c]$) can be adjusted through calibrating the bounds of the modulation and the duty cycle.

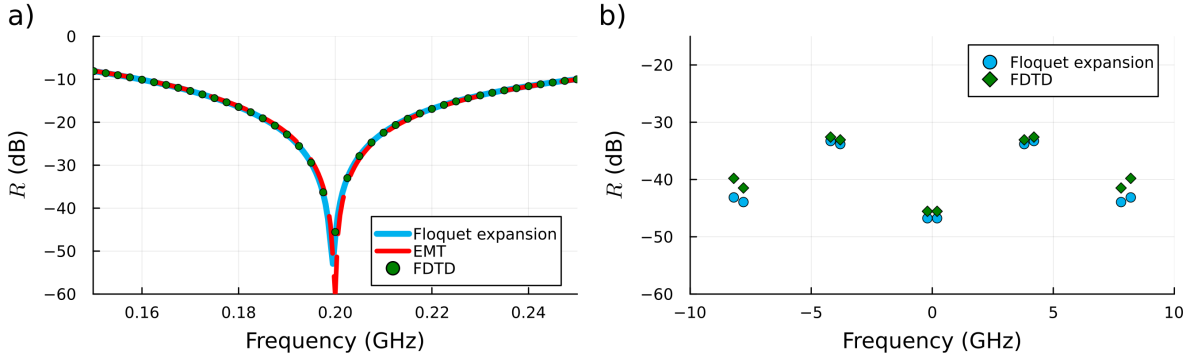


Figure 7: Reflectance of a grounded slab with passive permittivity modulation: a) Zeroth-order reflectance; b) reflectance of Floquet harmonics for $\omega_0 = 2\pi \cdot 0.2$ rad/ns.

Reflectance of the matched slab within the effective medium limit is given on Fig. 7; the modulation parameters were fixed to $T_e = 0.25$ ns, $\varepsilon_1 = 3.546$, $\varepsilon_2 = 4.28$, $\varepsilon_3 = 3.546$ and $\tau_{1e} = 0.55T_e$. The effective static response shows excellent agreement with both Floquet expansion and FDTD results, validating the use of passive switching for reconfigurable lossy materials. Reflectance of the first-order harmonics remains relatively small despite being higher than that of the zeroth-order harmonic. This discrepancy is largely governed by the relatively large modulation depth, which can be further relaxed by increasing the modulation frequency.

4 On the possibility of temporal uniaxial perfectly matched layers

Since the impedance-matched medium explored herein so far can only absorb TEM waves, a question arises on the applicability of the matching condition to a realistic slab configuration where the incident field can come from an arbitrary angle and in different polarizations. This problem has historically driven the development of a "true" PML medium for computational electromagnetics [35, 59, 60], as well as the quest for its realistic physical implementation [61, 62, 63]. Focusing solely on TE-polarized plane waves, the matching condition along the z -axis can be summarized as [59]:

$$\varepsilon_{xx} = \mu_{yy} = \frac{1}{\mu_{zz}} \quad (21)$$

where the constitutive parameters ε_{xx} and μ_{yy} are lossy. Evidently, this requires μ_{zz} to be active; it exhibits a magnetic Debye response with a negative coupling term and is expected to be unstable without the presence of loss in the transverse permittivity and permeabilities [61].

Owing to the linear time-variant nature of the materials considered herein, the usual matching condition needs to be reevaluated, which can be done so under the operator description of the constitutive

parameters under a Fourier basis [64, 65, 66]. Considering the problem of wave reflection from an interface between vacuum and an arbitrarily time-varying uniaxial medium as in [59, 60], we can write the dispersion relation of TE waves in the latter as (Appendix D):

$$\left[\hat{k}_0\hat{\mu}_{zz}\hat{k}_0\right]^{-1}\hat{k}_y^2 + \left[\hat{k}_0\hat{\mu}_{yy}\hat{k}_0\right]^{-1}\hat{k}_{zp}^2 = \hat{\varepsilon}_{xx} \quad (22)$$

where the hat symbol denotes the operator form. \hat{k}_y corresponds to the transverse wavevector, which is shared across the both half-spaces. In turn, \hat{k}_{zp} denotes the z -oriented wavevector in the uniaxial half-space. Per the reflection operator of time-varying half-spaces (Appendix B), complete admittance matching is achieved under the condition:

$$\hat{Y}_0 = \hat{Y}_p \quad (23)$$

where $\hat{Y}_0 = [\hat{\omega}\mu_0]^{-1}\hat{k}_{zi}$ and $\hat{Y}_p = [\hat{\omega}\mu_0\hat{\mu}_{yy}]^{-1}\hat{k}_{zp}$ are the admittance operators for multifrequency waves, $\hat{k}_0 = \hat{\omega}/c_0$ and $\hat{k}_{zi} = \left[\hat{k}_0^2 - \hat{k}_y^2\right]^{1/2}$; note that \hat{Y}_0 and \hat{k}_y are multiplication operators and correspond to diagonal matrices in matrix algebra, since the incident wave impinges from a linear time-invariant half-space. The exact matching requires:

$$\hat{k}_{zp} = \hat{k}_0\hat{\mu}_{yy}\hat{k}_0^{-1}\hat{k}_{zi} \quad (24)$$

Inserting Eq. 24 into Eq. 22 and noting that $\hat{k}_y^2 = \hat{k}_0^2 - \hat{k}_{zi}^2$, we obtain:

$$\hat{k}_0^{-1}\hat{\mu}_{zz}^{-1}\hat{k}_0 - \hat{k}_0^{-1}\hat{\mu}_{zz}^{-1}\hat{k}_0^{-1}\hat{k}_{zi}^2 + \hat{k}_0^{-2}\hat{k}_{zi}\hat{k}_0\hat{\mu}_{yy}\hat{k}_0^{-1}\hat{k}_{zi} = \hat{\varepsilon}_{xx} \quad (25)$$

It can be seen that the usual matching condition $\hat{\varepsilon}_{xx} = \hat{\mu}_{yy} = \hat{\mu}_{zz}^{-1}$ is guaranteed to exactly satisfy the dispersion equation for an arbitrary \hat{k}_{zi} only when the waves are normally incident ($\hat{k}_{zi} = \hat{k}_0$) or when the constitutive parameters are commuting multipliers, i.e. under a linear time-invariant material response. While the non-commutativity of these operators under arbitrary time-modulation does not preclude the existence of matched absorption at arbitrary angles, it implies that such conditions are fundamentally frequency- and modulation-dependent, potentially leading to inexact matching for Floquet harmonics. Thus, two-dimensional impedance matching may necessitate the use of active components alongside inverse-designed modulation profiles [67].

5 Conclusion

In conclusion, it is demonstrated that a temporal metamaterial can be engineered to behave as a PML-like matched absorber under passive modulation of the constitutive parameters. An effective medium model identifies modulation-dependent dielectric and magnetic losses in the quasistatic limit, which can be tuned to achieve reconfigurable operation. Beyond the planar transmission line configuration, these switched metamaterials can be constructed in the form of stacked metasurfaces as in [68], using programmable capacitors and high-frequency switches to obtain complex material responses. With the recent advances in the temporal permeability modulation of ferromagnetic materials at microwave frequencies [69], the absorption scheme can possibly be implemented in bulk metamaterials as well. While optical implementation of this PML-like matched absorption is complicated by the lack of intrinsic magnetic material responses in these frequencies, the proposed mechanism can still be emulated using graphene-based metamaterials under passive carrier injection [70].

Acknowledgments

The author thanks Prof. M. I. Aksun for useful discussions and guidance.

Appendix

A Transfer matrix method

Temporally-discrete and spatially-infinite media are most effectively analyzed using the transfer-matrix method (TMM) [2]. For the sake of brevity, only the derivation for the passive and synchronized PTCs is documented. Modulation functions for a two-phase and homogeneous time-periodic medium can be written as:

$$\varepsilon(t) = \begin{cases} \varepsilon_1, & n(\tau_1 + \tau_2) < t < n(\tau_1 + \tau_2) + \tau_1, \\ \varepsilon_2, & n(\tau_1 + \tau_2) - \tau_2 < t < n(\tau_1 + \tau_2), \end{cases} \quad (26)$$

$$\mu(t) = \begin{cases} \mu_1, & n(\tau_1 + \tau_2) < t < n(\tau_1 + \tau_2) + \tau_1, \\ \mu_2, & n(\tau_1 + \tau_2) - \tau_2 < t < n(\tau_1 + \tau_2), \end{cases} \quad (27)$$

for $n \in \mathbb{Z}$. Under the assumption of $\varepsilon_2 \geq \varepsilon_1$ and $\mu_2 \geq \mu_1$, the following definitions of the transfer matrix elements are employed for a fixed wavenumber k [71]:

$$M_{21} = \begin{bmatrix} t_{21}^{D,B} & r_{21}^{D,B} \\ r_{21}^{D,B} & t_{21}^{D,B} \end{bmatrix} \quad (28)$$

$$M_{12} = \begin{bmatrix} t_{12}^{E,H} & r_{12}^{E,H} \\ r_{12}^{E,H} & t_{12}^{E,H} \end{bmatrix} \quad (29)$$

$$P_1 = \begin{bmatrix} e^{-i\frac{kc_0}{\sqrt{\varepsilon_1\mu_1}}\tau_1} & 0 \\ 0 & e^{i\frac{kc_0}{\sqrt{\varepsilon_1\mu_1}}\tau_1} \end{bmatrix} \quad (30)$$

$$P_2 = \begin{bmatrix} e^{-i\frac{kc_0}{\sqrt{\varepsilon_2\mu_2}}\tau_2} & 0 \\ 0 & e^{i\frac{kc_0}{\sqrt{\varepsilon_1\mu_1}}\tau_2} \end{bmatrix} \quad (31)$$

where the reflection and transmissions coefficients r and t are found either for flux continuity for rising edges (D, B) or field continuity for falling edges (E, H) [72, 52]:

$$r_{21}^D = \frac{1}{2} \left[\frac{\varepsilon_1}{\varepsilon_2} - \sqrt{\frac{\varepsilon_1\mu_1}{\varepsilon_2\mu_2}} \right] \quad (32)$$

$$t_{21}^D = \frac{1}{2} \left[\frac{\varepsilon_1}{\varepsilon_2} + \sqrt{\frac{\varepsilon_1\mu_1}{\varepsilon_2\mu_2}} \right] \quad (33)$$

$$r_{12}^E = \frac{1}{2} \left[1 - \sqrt{\frac{\mu_1\varepsilon_2}{\mu_2\varepsilon_1}} \right] \quad (34)$$

$$t_{12}^E = \frac{1}{2} \left[1 + \sqrt{\frac{\mu_1\varepsilon_2}{\mu_2\varepsilon_1}} \right] \quad (35)$$

Having defined the transfer functions, we can obtain the band diagram from the following eigenproblem:

$$P_1 M_{21} P_2 M_{12} \begin{bmatrix} E^+ \\ E^- \end{bmatrix} = e^{-i\omega(\tau_1+\tau_2)} \begin{bmatrix} E^+ \\ E^- \end{bmatrix} \quad (36)$$

For the specific case of impedance-matched modulation with $\varepsilon_1 = \mu_1$ and $\mu_1 = \mu_2$, the eigenproblem can be written as:

$$P_1 M_{21} P_2 M_{12} \begin{bmatrix} E^+ \\ E^- \end{bmatrix} = \begin{bmatrix} \frac{\varepsilon_1}{\varepsilon_2} e^{-ikc_0\left(\frac{\tau_1}{\varepsilon_1} + \frac{\tau_2}{\varepsilon_2}\right)} & 0 \\ 0 & \frac{\varepsilon_1}{\varepsilon_2} e^{ikc_0\left(\frac{\tau_1}{\varepsilon_1} + \frac{\tau_2}{\varepsilon_2}\right)} \end{bmatrix} \begin{bmatrix} E^+ \\ E^- \end{bmatrix} = e^{-i\omega(\tau_1+\tau_2)} \begin{bmatrix} E^+ \\ E^- \end{bmatrix} \quad (37)$$

Thus, the dispersion relation can be reduced to Eq. 10.

B Floquet expansion method

Since the temporal modulation considered herein is purely periodic, the reflection of electromagnetic waves from a time-variant isotropic slab of length d can be calculated semi-analytically through Floquet expansion [2] within an operator formalism [64, 65, 66]. Under this approach, standard scalar wave parameters can be replaced by equivalent operator expressions that act on the spectrum of the electromagnetic fields. This enables the robust time-harmonic representation of multi-frequency coupling in a matrix form within the Floquet basis, resulting in expressions similar to those in [47]. For instance, double-time convolution involving a dynamic susceptibility function can be represented in the operator form as:

$$\mathbf{P}(t) = \varepsilon_0 \int_{-\infty}^{\infty} dt' \chi(t, t - t') \mathbf{E}(t') \rightarrow \mathbf{P} = \varepsilon_0 \hat{\chi} \mathbf{E} \quad (38)$$

where the hat symbol denotes the operator (or matrix) form. It is worth noting that an antinormal-like operator ordering has been assumed [64].

It is assumed that a time-variant slab of thickness d is grounded at $z = d$ with a perfect electrical conductor; a y -polarized incident plane wave that is traveling in z -direction impinges on the structure. Consequently, the transverse fields in the space below (1) and within the slab (2) can be written as [64]:

$$E_x^{(1)} = e^{i\hat{k}_{z1}z} + e^{-i\hat{k}_{z1}z} \hat{\Gamma}, \quad (z \geq 0) \quad (39)$$

$$E_x^{(2)} = e^{i\hat{k}_{z2}z} \hat{A} + e^{-i\hat{k}_{z2}z} \hat{B}, \quad (z < 0) \quad (40)$$

$$H_y^{(1)} = \hat{Y}_1 \left[e^{i\hat{k}_{z1}z} - e^{-i\hat{k}_{z1}z} \hat{\Gamma} \right], \quad (z \geq 0) \quad (41)$$

$$H_y^{(2)} = \hat{Y}_2 \left[e^{i\hat{k}_{z2}z} \hat{A} - e^{-i\hat{k}_{z2}z} \hat{B} \right], \quad (z < 0) \quad (42)$$

where $\hat{Y}_n = [\hat{\omega} \mu_0 \hat{\mu}_c]^{-1} \hat{k}_{zn}$ is the admittance operator and $\hat{k}_{zn} = [\hat{\omega} \hat{\mu}_c \hat{\omega} \hat{\varepsilon}_c (\mu_0 \varepsilon_0) - k_x^2 I]^{1/2}$ is the transverse wavevector operator for a fixed k_x vector. $\hat{\varepsilon}_c$ and $\hat{\mu}_c$ are the complex permittivity and permeability operators:

$$\hat{\varepsilon}_c = \hat{\varepsilon} + i\hat{\omega}^{-1} \varepsilon_0^{-1} \hat{\sigma} \quad (43)$$

$$\hat{\mu}_c = \hat{\mu} + i\hat{\omega}^{-1} \mu_0^{-1} \hat{\sigma}^* \quad (44)$$

with $\hat{\sigma}$ and $\hat{\sigma}^*$ being electric and magnetic conductivity operators. These are practically constructed in the form of Toeplitz matrices using fast Fourier transform of the time-domain waveforms, with the conductivity profiles being obtained from Eqs. 5 to 8. At $z = d$ perfect conductor boundary conditions are applied:

$$E_x^{(2)} = e^{i\hat{k}_{z2}d} \hat{A} + e^{-i\hat{k}_{z2}d} \hat{B} = 0 \quad (45)$$

$$\hat{B} = -e^{i\hat{k}_{z2}2d} \hat{A} \quad (46)$$

Enforcing the field continuity at $z = 0$,

$$I + \hat{\Gamma} = \hat{A} + \hat{B} = \left[I - e^{i\hat{k}_{z2}2d} \right] \hat{A} \quad (47)$$

$$\hat{Y}_1 \left[I - \hat{\Gamma} \right] = \hat{Y}_2 \left[\hat{A} - \hat{B} \right] = \hat{Y}_2 \left[I + e^{i\hat{k}_{z2}2d} \right] \hat{A} \quad (48)$$

Algebraic manipulation of the expressions above yields the reflection operator for the grounded slab:

$$\hat{\Gamma} = \left[\hat{Y}_1 + \hat{Y}_2 \hat{X} \right]^{-1} \left[\hat{Y}_1 - \hat{Y}_2 \hat{X} \right] \quad (49)$$

where $\hat{X} = \left[I + e^{i\hat{k}_{z2}2d} \right] \left[I - e^{i\hat{k}_{z2}2d} \right]^{-1}$. The reflection coefficient for the time-modulated half-space can be retrieved for the limit of an infinitely-thick slab:

$$\hat{\Gamma}_0 = \lim_{d \rightarrow \infty} \hat{\Gamma} = \left[\hat{Y}_1 + \hat{Y}_2 \right]^{-1} \left[\hat{Y}_1 - \hat{Y}_2 \right] \quad (50)$$

It is worth highlighting that for this specific case, the matrix square root should be computed in a way to enforce radiation condition at infinity [64], which is done here with Schur method [73]. While the calculations herein were performed for isotropic materials, the expressions themselves are valid for uniaxial slabs that support TE modes, as long as the corresponding wavenumber and admittance operators are derived using the appropriate dispersion relation (Appendix D).

C FDTD simulations

Update equations for the 1D FDTD simulations are given as [74, 75]:

$$E_x^{n+1}(i) = \left[\frac{\varepsilon^n(i) - \frac{\sigma(i)\Delta t}{2\varepsilon_0}}{\varepsilon^{n+1}(i) + \frac{\sigma(i)\Delta t}{2\varepsilon_0}} \right] E_x^n(i) - \frac{\Delta t}{\Delta z \varepsilon_0} \left[\frac{1}{\varepsilon^{n+1}(i) + \frac{\sigma(i)\Delta t}{2\varepsilon_0}} \right] \times \left[H_y^{n+0.5} \left(i + \frac{1}{2} \right) - H_y^{n+0.5} \left(i - \frac{1}{2} \right) \right] \quad (51)$$

$$H_y^{n+0.5} \left(i + \frac{1}{2} \right) = \left[\frac{\mu^{n-0.5}(i+0.5) - \frac{\sigma^*(i+0.5)\Delta t}{2\mu_0}}{\mu^{n+0.5}(i+0.5) + \frac{\sigma^*(i+0.5)\Delta t}{2\mu_0}} \right] H_y^{n-0.5} \left(i + \frac{1}{2} \right) - \frac{\Delta t}{\Delta z \mu_0} \left[\frac{1}{\mu^{n+1}(i) + \frac{\sigma^*(i)\Delta t}{2\mu_0}} \right] [E_x^n(i+1) - E_x^n(i)] \quad (52)$$

where σ and σ^* are the tapered magnetic conductivities to enforce PMLs. Δt and Δz correspond to temporal and spatial step sizes, respectively. The simulation region is terminated at both ends with perfect conductor boundaries. Since standard update equations for nondispersive temporal modulation naturally enforce the continuity of \mathbf{D} and \mathbf{B} [76], the following corrections are applied on the field components at the falling edges of time-dependent permittivity and permeability functions ($\varepsilon^{n+1} < \varepsilon^n$ or $\mu^{n+0.5} < \mu^{n-0.5}$):

$$\tilde{E}_x^{n+1}(i) = \frac{\varepsilon^{n+1}(i)}{\varepsilon^n(i)} E_x^{n+1}(i) \quad (53)$$

$$\tilde{H}_y^{n+0.5} \left(i + \frac{1}{2} \right) = \frac{\mu^{n+0.5} \left(i + \frac{1}{2} \right)}{\mu^{n-0.5} \left(i + \frac{1}{2} \right)} H_y^{n+0.5} \left(i + \frac{1}{2} \right) \quad (54)$$

D Waves in time-varying uniaxial media

Under the operator formalism (Appendix B), Maxwell's equations under TE polarization for an arbitrarily time-varying uniaxial media can be written as:

$$\frac{dE_x}{dy} = -i\hat{\omega}\mu_0\hat{\mu}_{zz}H_z \quad (55)$$

$$\frac{dE_x}{dz} = i\hat{\omega}\mu_0\hat{\mu}_{yy}H_y \quad (56)$$

$$\frac{dH_z}{dy} - \frac{dH_y}{dz} = -i\hat{\omega}\varepsilon_0\hat{\varepsilon}_{xx}E_x \quad (57)$$

where $-i\hat{\omega}$, $\hat{\varepsilon}$ and $\hat{\mu}$ are the derivative, permittivity and permeability operators, respectively. The media is assumed to be translationally-invariant along the x -axis. Substituting Eqs. 55 and 56 into Eq. 57, and seeking out plane wave solutions ($E_x \propto e^{i\hat{k}_y y + i\hat{k}_z z}$), we obtain:

$$\frac{d}{dy} \left([-i\hat{\omega}\hat{\mu}_0\hat{\mu}_{zz}]^{-1} \frac{dE_x}{dy} \right) - \frac{d}{dz} \left([i\hat{\omega}\hat{\mu}_0\hat{\mu}_{yy}]^{-1} \frac{dE_x}{dz} \right) = -i\hat{\omega}\varepsilon_0\hat{\varepsilon}_{xx}E_x \quad (58)$$

$$\left([\hat{\omega}\hat{\mu}_0\hat{\mu}_{zz}]^{-1} \hat{k}_y^2 - [\hat{\omega}\hat{\mu}_0\hat{\mu}_{yy}]^{-1} \hat{k}_z^2 \right) E_x = \hat{\omega}\varepsilon_0\hat{\varepsilon}_{xx}E_x \quad (59)$$

with $\hat{k}_{y,z}$ being the wavevector operators. Dividing both sides by $\hat{\omega}\varepsilon_0$ and defining the wavenumber operator as $\hat{k}_0 = \hat{\omega}\sqrt{\varepsilon_0\mu_0}$, the dispersion relation of plane waves in uniaxial time-varying media is derived:

$$\left[\hat{k}_0\hat{\mu}_{zz}\hat{k}_0 \right]^{-1} \hat{k}_y^2 + \left[\hat{k}_0\hat{\mu}_{yy}\hat{k}_0 \right]^{-1} \hat{k}_z^2 = \hat{\varepsilon}_{xx} \quad (60)$$

References

- [1] M. H. Mostafa, M. S. Mirmoosa, M. S. Sidorenko, V. S. Asadchy, and S. A. Tretyakov. Temporal interfaces in complex electromagnetic materials: an overview. *Opt. Mater. Express*, 14(5):1103, April 2024.
- [2] Mohammad M. Asgari, Puneet Garg, Xuchen Wang, Mohammad S. Mirmoosa, Carsten Rockstuhl, and Viktor Asadchy. Theory and applications of photonic time crystals: a tutorial. *Adv. Opt. Photon.*, 16(4):958, November 2024.
- [3] Alireza Akbarzadeh, Nima Chamanara, and Christophe Caloz. Inverse prism based on temporal discontinuity and spatial dispersion. *Opt. Lett.*, 43(14):3297, July 2018.
- [4] Romain Tirole, Stefano Vezzoli, Emanuele Galiffi, Iain Robertson, Dries Maurice, Benjamin Tilmann, Stefan A. Maier, John B. Pendry, and Riccardo Sapienza. Double-slit time diffraction at optical frequencies. *Nat. Phys.*, 19(7):999–1002, April 2023.
- [5] Victor Pacheco-Peña and Nader Engheta. Temporal aiming. *Light Sci. Appl.*, 9(1), July 2020.
- [6] Victor Pacheco-Peña and Nader Engheta. Antireflection temporal coatings. *Optica*, 7(4):323, April 2020.
- [7] L. Felsen and G. Whitman. Wave propagation in time-varying media. *IEEE Trans. Antennas Propag.*, 18(2):242–253, March 1970.
- [8] N. S. Stepanov. Dielectric constant of unsteady plasma. *Radiophys. Quantum Electron.*, 19(7):683–689, July 1976.
- [9] Dikshitulu K. Kalluri. *Electromagnetics of Time Varying Complex Media: Frequency and Polarization Transformer*. CRC Press, Boca Raton, FL, 2018.
- [10] Huanan Li, Shixiong Yin, and Andrea Alù. Nonreciprocity and Faraday rotation at time interfaces. *Phys. Rev. Lett.*, 128(17), April 2022.
- [11] Božidar V. Stanić. Electromagnetic waves in a suddenly created Lorentz medium and plasma. *J. Appl. Phys.*, 70(4):1987–1990, August 1991.
- [12] Diego M. Solís, Raphael Kastner, and Nader Engheta. Time-varying materials in the presence of dispersion: plane-wave propagation in a Lorentzian medium with temporal discontinuity. *Photonics Res.*, 9(9):1842, August 2021.

- [13] M. I. Bakunov, A. V. Shirokova, and A. V. Maslov. Constitutive relations and adiabatic invariants for electromagnetic waves in a dynamic Lorentz medium. *Phys. Rev. B*, 104(3), July 2021.
- [14] M. I. Bakunov, A. V. Shirokova, M. A. Kurnikov, and A. V. Maslov. Light scattering at a temporal boundary in a Lorentz medium. *Opt. Lett.*, 46(19):4988, September 2021.
- [15] M. I. Bakunov, A. V. Shirokova, M. A. Kurnikov, and A. V. Maslov. Electromagnetic waves in a Lorentzian medium with periodically modulated oscillator density. *Phys. Rev. A*, 110(6), December 2024.
- [16] Shixiong Yin, Yao-Ting Wang, and Andrea Alù. Temporal optical activity and chiral time-interfaces. *Opt. Express*, 30(26):47933, December 2022.
- [17] Mohamed Hesham Mohamed Mostafa, Mohammad S. Mirmoosa, and Sergei A. Tretyakov. Spin-dependent phenomena at chiral temporal interfaces. *Nanophotonics*, 12(14):2881–2889, March 2023.
- [18] Grigorii Ptitsyn, Diego M. Solís, Mohammad Sajjad Mirmoosa, and Nader Engheta. Temporal interface in dispersive hyperbolic media. *Nanophotonics*, 14(23):4207–4218, August 2025.
- [19] Mikhail Sidorenko, Sergei Tretyakov, and Constantin Simovski. Temporal interface in wire media: Generation of multiple waves. *Phys. Rev. B*, 112(23), December 2025.
- [20] Constantin Simovski, Mohammad Sajjad Mirmoosa, Mikhail Sidorenko, and Sergei Tretyakov. Electromagnetic time interfaces in wire media: Innovations for subwavelength imaging. *Phys. Rev. Research*, 7(3), August 2025.
- [21] Victor Pacheco-Peña, Yasaman Kiasat, Diego M. Solís, Brian Edwards, and Nader Engheta. Holding and amplifying electromagnetic waves with temporal non-Foster metastructures. *Nat. Comm.*, 16(1), March 2025.
- [22] Hady Moussa, Gengyu Xu, Shixiong Yin, Emanuele Galiffi, Younes Ra'di, and Andrea Alù. Observation of temporal reflection and broadband frequency translation at photonic time interfaces. *Nat. Phys.*, 19(6):863–868, March 2023.
- [23] Thomas R. Jones, Alexander V. Kildishev, Mordechai Segev, and Dimitrios Peroulis. Time-reflection of microwaves by a fast optically-controlled time-boundary. *Nat. Commun.*, 15(1), August 2024.
- [24] Tom A Kuusela. Time mirror in a lumped transmission line. *Eur. J. Phys.*, 46(4):045204, July 2025.
- [25] Haonan Hou, Kai Peng, Yangkai Wang, Jiarui Wang, Xudong Zhang, Ren Wang, Hao Hu, and Jiang Xiong. Experimental realization of a full-band wave antireflection based on temporal taper metamaterials. *Commun. Phys.*, 9(1), January 2026.
- [26] Yiyu Zhou, M. Zahirul Alam, Mohammad Karimi, Jeremy Upham, Orad Reshef, Cong Liu, Alan E. Willner, and Robert W. Boyd. Broadband frequency translation through time refraction in an epsilon-near-zero material. *Nat. Commun.*, 11(1), May 2020.
- [27] Eran Lustig, Ohad Segal, Soham Saha, Eliyahu Bordo, Sarah N. Chowdhury, Yonatan Sharabi, Avner Fleischer, Alexandra Boltasseva, Oren Cohen, Vladimir M. Shalaev, and Mordechai Segev. Time-refraction optics with single cycle modulation. *Nanophotonics*, 12(12):2221–2230, May 2023.
- [28] Brian L. Kim, Christopher Chong, and Chiara Daraio. Temporal refraction in an acoustic phononic lattice. *Phys. Rev. Lett.*, 133(7), August 2024.
- [29] Benjamin Apffel and Emmanuel Fort. Frequency conversion cascade by crossing multiple space and time interfaces. *Phys. Rev. Lett.*, 128(6), February 2022.

- [30] M. I. Bakunov and A. V. Maslov. Reflection and transmission of electromagnetic waves at a temporal boundary: comment. *Opt. Lett.*, 39(20):6029, October 2014.
- [31] Emanuele Galiffi, Diego Martínez Solís, Shixiong Yin, Nader Engheta, and Andrea Alù. Electrodynamics of photonic temporal interfaces. *Light Sci. Appl.*, 14(1), September 2025.
- [32] A. V. Maslov. Wave transformation in transmission lines with rapid connection and disconnection of reactive elements. *J. Appl. Phys.*, 137(1), January 2025.
- [33] Hossein Mehrpour Bernety, Dikshitulu K. Kalluri, and Mark A. Cappelli. Proper treatment of energy and momentum in time-modulated plasmas. *Phys. Rev. E*, 113:025204, Feb 2026.
- [34] Shixiong Yin and Andrea Alù. Passive photonic time crystals. In *Metamaterials, Metadevices, and Metasystems 2024*, page 23. SPIE, October 2024.
- [35] Jean-Pierre Berenger. A perfectly matched layer for the absorption of electromagnetic waves. *J. Comput. Phys.*, 114(2):185–200, October 1994.
- [36] Jun-Rui Pan and Hai-Feng Zhang. Broadband absorption phenomena in temporal metamaterials with modulation of the refractive index. *Appl. Opt.*, 64(25):7558, August 2025.
- [37] Amir Shlivinski and Yakir Hadad. Beyond the Bode-Fano bound: Wideband impedance matching for short pulses using temporal switching of transmission-line parameters. *Phys. Rev. Lett.*, 121(20), November 2018.
- [38] Huanan Li and Andrea Alù. Temporal switching to extend the bandwidth of thin absorbers. *Optica*, 8(1):24, December 2020.
- [39] Chen Firestein, Amir Shlivinski, and Yakir Hadad. Absorption and scattering by a temporally switched lossy layer: Going beyond the Rozanov bound. *Phys. Rev. Appl.*, 17(1), January 2022.
- [40] Xiaozhen Yang, Erda Wen, and Daniel F. Sievenpiper. Broadband time-modulated absorber beyond the Bode-Fano limit for short pulses by energy trapping. *Phys. Rev. Appl.*, 17(4), April 2022.
- [41] Suwun Suwunnarat, Dashiell Halpern, Huanan Li, Boris Shapiro, and Tsampikos Kottos. Dynamically modulated perfect absorbers. *Phys. Rev. A*, 99(1), January 2019.
- [42] Emanuele Galiffi, Gengyu Xu, Shixiong Yin, Hady Moussa, Younes Ra’di, and Andrea Alù. Broadband coherent wave control through photonic collisions at time interfaces. *Nat. Phys.*, 19(11):1703–1708, August 2023.
- [43] Emanuele Galiffi, Anthony C. Harwood, Stefano Vezzoli, Romain Tirole, Andrea Alù, and Riccardo Sapienza. Optical coherent perfect absorption and amplification in a time-varying medium. *Nat. Photon.*, January 2026.
- [44] B. Chambers and A. Tennant. A smart radar absorber based on the phase-switched screen. *IEEE Trans. Antennas Propag.*, 53(1):394–403, January 2005.
- [45] M.H. Mostafa, A. Díaz-Rubio, M.S. Mirmoosa, and S.A. Tretyakov. Coherently time-varying metasurfaces. *Phys. Rev. Appl.*, 17(6), June 2022.
- [46] Zeki Hayran and Francesco Monticone. Beyond the Rozanov bound on electromagnetic absorption via periodic temporal modulations. *Phys. Rev. Appl.*, 21(4), April 2024.
- [47] Matteo Ciabattoni, Zeki Hayran, and Francesco Monticone. Observation of broadband super-absorption of electromagnetic waves through space-time symmetry breaking. *Sci. Adv.*, 11(3), January 2025.

- [48] Victor Pacheco-Peña and Nader Engheta. Effective medium concept in temporal metamaterials. *Nanophotonics*, 9(2):379–391, December 2019.
- [49] Dani Torrent. Strong spatial dispersion in time-modulated dielectric media. *Phys. Rev. B*, 102(21), December 2020.
- [50] Noyan Kinayman and M. I. Aksun. *Modern Microwave Circuits*. Artech House, Norwood, MA, 2005.
- [51] Shixiong Yin, Emanuele Galiffi, Gengyu Xu, and Andrea Alù. Scattering at temporal interfaces: An overview from an antennas and propagation engineering perspective. *IEEE Antennas Propag. Mag.*, 65(4):21–28, August 2023.
- [52] F.R. Morgenthaler. Velocity modulation of electromagnetic waves. *IRE Trans. Microw. Theory Tech.*, 6(2):167–172, April 1958.
- [53] José Gabriel Gaxiola-Luna and P. Halevi. Temporal photonic (time) crystal with a square profile of both permittivity $\varepsilon(t)$ and permeability $\mu(t)$. *Phys. Rev. B*, 103(14), April 2021.
- [54] Mariana Dalarsson, Balwan Rana, and Victor Pacheco-Peña. Space-harmonic approach to graded temporal metamaterials. *Opt. Mater. Express*, 15(6):1318, May 2025.
- [55] K. N. Rozanov. Ultimate thickness to bandwidth ratio of radar absorbers. *IEEE Trans. Antennas Propag.*, 48(8):1230–1234, 2000.
- [56] Chen Firestein, Amir Shlivinski, and Yakir Hadad. Sum rule bounds beyond Rozanov criterion in linear and time-invariant thin absorbers. *Phys. Rev. B*, 108(1), July 2023.
- [57] Stefanos Fr. Koufidis, Theodoros T. Koutserimpas, Francesco Monticone, and Martin W. McCall. Enhanced scattering from an almost-periodic optical temporal slab. *Phys. Rev. A*, 110(4), October 2024.
- [58] Patrick Kofod Mogensen and Asbjørn Nilsen Riseth. Optim: A mathematical optimization package for Julia. *J. Open Source Softw.*, 3(24):615, 2018.
- [59] Z.S. Sacks, D.M. Kingsland, R. Lee, and Jin-Fa Lee. A perfectly matched anisotropic absorber for use as an absorbing boundary condition. *IEEE Trans. Antennas Propag.*, 43(12):1460–1463, 1995.
- [60] S. D. Gedney. An anisotropic perfectly matched layer-absorbing medium for the truncation of FDTD lattices. *IEEE Trans. Antennas Propag.*, 44(12):1630–1639, December 1996.
- [61] R. W. Ziolkowski. The design of Maxwellian absorbers for numerical boundary conditions and for practical applications using engineered artificial materials. *IEEE Trans. Antennas Propag.*, 45(4):656–671, April 1997.
- [62] F. L. Teixeira. On aspects of the physical realizability of perfectly matched absorbers for electromagnetic waves. *Radio Sci.*, 38(2), February 2003.
- [63] C. A. Valagiannopoulos, J. Vehmas, C. R. Simovski, S. A. Tretyakov, and S. I. Maslovski. Electromagnetic energy sink. *Phys. Rev. B*, 92(24), December 2015.
- [64] S. A. R. Horsley, E. Galiffi, and Y.-T. Wang. Eigenpulses of dispersive time-varying media. *Phys. Rev. Lett.*, 130:203803, May 2023.
- [65] Calvin M. Hooper, James R. Capers, Ian R. Hooper, and Simon A. R. Horsley. Symmetry-protected lossless modes in dispersive time-varying media. *Phys. Rev. A*, 111(3), March 2025.

- [66] Suat Barış İplikçioğlu and M. I. Aksun. Analytical modeling of time-varying and dispersive metasurfaces with surface susceptibility operators. *Phys. Rev. B*, 111(24), June 2025.
- [67] Puneet Garg, Jan David Fischbach, Aristeidis G. Lampryanidis, Xuchen Wang, Mohammad S. Mirmoosa, Viktor S. Asadchy, Carsten Rockstuhl, and Thomas J. Sturges. Inverse-designed dispersive time-varying nanostructures. *Adv. Opt. Mater.*, 13(5), January 2025.
- [68] Mostafa Movahediqomi, Sergei Tretyakov, Viktor Asadchy, and Xuchen Wang. Stacked time-varying metasurfaces. *Adv. Opt. Mater.*, 14(4), January 2026.
- [69] Toshiyuki Kodama, Nobuaki Kikuchi, Satoshi Okamoto, Seigo Ohno, and Satoshi Tomita. Spin-current-driven permeability variation for time-varying magnetic metamaterials. *Phys. Rev. Appl.*, 19(4), April 2023.
- [70] A. V. Maslov and M. I. Bakunov. Temporal scattering of a graphene plasmon by a rapid carrier density decrease. *Optica*, 5(12):1508, November 2018.
- [71] D. Ramaccia, A. Alù, A. Toscano, and F. Bilotti. Temporal multilayer structures for designing higher-order transfer functions using time-varying metamaterials. *Appl. Phys. Lett.*, 118(10), March 2021.
- [72] Yuzhe Xiao, Drew N. Maywar, and Govind P. Agrawal. Reflection and transmission of electromagnetic waves at a temporal boundary. *Opt. Letters*, 39(3):574, January 2014.
- [73] Åke Björck and Sven Hammarling. A Schur method for the square root of a matrix. *Linear Algebra Its Appl.*, 52–53:127–140, July 1983.
- [74] Allen Taflov and Susan C. Hagness. *Computational Electrodynamics: the Finite-Difference Time-Domain Method*. Artech House, Norwood, MA, 3rd edition, 2005.
- [75] Xiaowen Liu and Derek A. McNamara. The use of the FDTD method for electromagnetic analysis in the presence of independently time-varying media. *Int. J. Infrared Milli. Waves*, 28(9):759–778, June 2007.
- [76] Amir Bahrami, Zoé-Lise Deck-Léger, Zhiyu Li, and Christophe Caloz. A generalized FDTD scheme for moving electromagnetic structures with arbitrary space–time configurations. *IEEE Trans. Antennas Propag.*, 72(2):1721–1734, February 2024.